Chemical Science

ROYAL SOCIETY OF CHEMISTRY

EDGE ARTICLE

View Article Online
View Journal | View Issue

Cite this: *Chem. Sci.*, 2021, **12**, 8468

All publication charges for this article have been paid for by the Royal Society of Chemistry

Quantitative interrogation of protein co-aggregation using multi-color fluorogenic protein aggregation sensors†

Yulong Bai,[ab] Wang Wan,*[a] Yanan Huang,[a] Wenhan Jin,[a] Haochen Lyu,[a] Qiuxuan Xia,[ab] Xuepeng Dong,[c] Zhenming Gao[c] and Yu Liu *[a]

Received 25th February 2021
Accepted 19th May 2021

DOI: 10.1039/d1sc01122g

rsc.li/chemical-science

Co-aggregation of multiple pathogenic proteins is common in neurodegenerative diseases but deconvolution of such biochemical process is challenging. Herein, we developed a dual-color fluorogenic thermal shift assay to simultaneously report on the aggregation of two different proteins and quantitatively study their thermodynamic stability during co-aggregation. Expansion of spectral coverage was first achieved by developing multi-color fluorogenic protein aggregation sensors. Orthogonal detection was enabled by conjugating sensors of minimal fluorescence crosstalk to two different proteins *via* sortase-tag technology. Using this assay, we quantified shifts in melting temperatures in a heterozygous model protein system, revealing that the thermodynamic stability of wild-type proteins was significantly compromised by the mutant ones but not *vice versa*. We also examined how small molecule ligands selectively and differentially interfere with such interplay. Finally, we demonstrated these sensors are suited to visualize how different proteins exert influence on each other upon their co-aggregation in live cells.

Introduction

Nascent polypeptides fold into defined structures to acquire their biological functions.[1] Though the folding processes of most proteins are naturally evolved to be energetically favourable, the thermodynamic and kinetic stabilities of a protein are frequently compromised by cellular stresses, genetic mutations, and exogenous chemical modifications.[2] Decreased protein stability leads to its misfolding, aggregation, and degradation. Numerous human diseases have been associated with aberrant protein aggregation, including Alzheimer's disease, Parkinson's disease, amyotrophic lateral sclerosis, and familiar amyloidosis.[3–5] Multiple lines of biological and pathological evidence have confirmed the co-aggregation behaviours of different pathogenic proteins, such as amyloid β and Tau in Alzheimer's disease.[6–9] Depicting the co-aggregation process is essential to delineate the disease mechanism and identify authentic drug target. However, it has always been a technical challenge to monitor different proteins' aggregation during the co-aggregation process.

Much light has been shed on developing sensors and analytical methods to study protein aggregation both *in vitro* and *in vivo*.[10,11] Fluorescence based methods have been widely explored due to their general applicability, flexibility, and robustness. Organic environment-sensitive dyes, including solvatochromic fluorophores,[12,13] fluorescent molecular rotors,[14–16] and aggregation induced emission (AIEgen) probes,[17–19] can sense the micro-environmental changes upon protein aggregation. These sensors are exemplified by Thioflavin T,[20] carbazoles,[21] polythiophenes,[22] and BODIPY.[23] In particular, AIEgens developed by Tang,[17,18] Zhu,[19] Hong[24,25] *et al.* report on amyloid aggregates or unfolded proteins. Materials based reagents, like luminescent polymers, nanoparticles, or quantum dots, broadened the chemical space for amyloid sensors.[26] Meade,[27] Mirica[28] and Marti[29] *et al.* filled in the gap of organic sensors and inorganic materials by using organometallic complexes to probe amyloid proteins. To further resolve the misfolded and aggregated ensembles, single molecule fluorescence based assay was developed by Deniz *et al.* to directly detect conformational subpopulations and their dynamics.[30–32] In addition, mass spectrometry based methods developed by Englander[33–36] and Robinson[37–40] provided mechanistic insights at residual resolution.

However, most of the protein aggregation detection methods abovementioned are limited to single protein investigation and hardly resolve the co-aggregation process of different proteins.

[a]*CAS Key Laboratory of Separation Science for Analytical Chemistry, Dalian Institute of Chemical Physics, Chinese Academy of Sciences, 457 Zhongshan Road, Dalian 116023, China. E-mail: liuyu@dicp.ac.cn; wanwang@dicp.ac.cn*

[b]*University of Chinese Academy of Sciences, Beijing 100049, China*

[c]*The Second Hospital of Dalian Medical University, 467 Zhongshan Road, Dalian, 116044, China*

† Electronic supplementary information (ESI) available: Supplemental figures, experimental method section, synthetic methods and schemes and NMR spectra. See DOI: 10.1039/d1sc01122g

Towards this end, series of conventional bioanalytical methods have been exploited to capture snapshots of this process, such as co-immunoprecipitation, chromatography, and differential centrifugation. Biosensors enabled cell imaging techniques (fluorescence resonance energy transfer (FRET) or fluorescence correlation spectroscopy (FCS)) extended the study into cellular mileu.[41,42] Towards intact and quantitative interrogation of protein co-aggregation process, Radford *et al.* pioneered in developing advanced mass spectrometry methods and provided unprecedented resolution in detecting the interplay of co-aggregation kinetics.[6]

While most of the previous works focused on aggregation kinetics, we aimed to quantitatively study the interplay of the thermodynamic stability between different proteins during their co-aggregation process. Thermal shift assay is widely utilized in the pharmaceutical industry to evaluate protein thermodynamic stability and its change upon ligand binding due to its facile fluorescence readout, quantitative result, and high throughput nature.[43–46] In particular, cellular thermal shift assay combined with proteomics has demonstrated its power in cellular drug-target engagement studies.[47,48] However, current assay relies on a solvatochromic fluorophore SYPRO® orange[49–51] or a fluorescent molecular rotor PROTEOSTAT®[52–54] that reports on protein unfolding and aggregation (Fig. 1a), thus only suitable for single-protein analysis.

Herein, we created a dual-color thermal shift assay (TSA) that orthogonally and quantitatively monitors two different proteins' co-aggregation process (Fig. 1b). Petersson *et al.* exemplified bioorthogonal conjugation of a sensor to the protein target allowed for selective detection of protein conformational changes.[55–57] Zhang *et al.* introduced chemical tag strategy to the field, enabling visualization of aggregation process of a specific protein-of-interest in live cells.[58–62] Inspired by these seminal works, through sortase mediated site specific bio-conjugation, we first demonstrated four environment-sensitive fluorophores with spectral coverage from 500 nm to 620 nm can serve as protein aggregation sensors. Two of these sensors (CCVJ and Mero) exhibited minimal fluorescence crosstalk and detected the co-aggregation of two different proteins. Unlike other aggregation sensors only reporting on the late-stage species, our sensors detected early misfolded soluble oligomers. In contrast to the single-color thermal shift assay, our method revealed how mutant proteins of destabilized thermodynamic stability compromise the wild type ones during the co-aggregation process in a heterozygous system but not *vice versa*. Small molecule ligands exerted differential and selective influences on different proteins during their co-aggregation. Finally, we extended our study to the cellular milieu to detect protein co-aggregation in live cells.

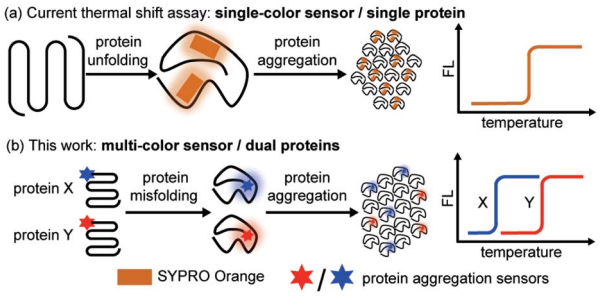

Fig. 1 Dual-color thermal shift assay simultaneously detects the co-aggregation of two proteins and quantify the changes in the thermodynamic stability, revealing their interplay. (a) Current thermal shift assay utilizes SYPRO® orange probe to detect single-protein aggregation *via* one-color fluorescence readout. (b) In this work, a dual-color thermal shift assay was developed to monitor dual-protein co-aggregation simultaneously *via* two orthogonal fluorescence readouts. Protein aggregation sensors were conjugated to the protein-of-interest *via* sortase-tag.

Results and discussion

Environment-sensitive fluorophores serve as protein aggregation sensor

The key to simultaneously monitor the aggregation of different proteins using our proposed multi-color thermal shift assay (Fig. 1b) is the orthogonal fluorescence signal readouts with minimal crosstalk. Such crosstalk usually arises from fluorescence resonance energy transfer (FRET) due to spectral overlaps and spatial proximity after aggregation. To minimize the FRET effect, we first expanded the spectral coverage of fluorogenic sensors to detect protein aggregation. Protein phase separation that involves protein unfolding, misfolding, and aggregation often accompanies with changes in the polarity and viscosity of local micro-environment.[25] Thus, fluorophores of polarity or viscosity sensitivity are potential candidates as protein aggregation sensors. Four environment-sensitive fluorophores were selected based on their environment-sensitive fluorogenicity reported in literatures (Fig. 2a), including CCVJ[63] (Fig. S1,† a fluorescent molecular rotor sensitive to viscosity), DCDHF[64,65] (Fig. S2,† a fluorescent molecular rotor sensitive to viscosity), RFP[59,66,67] (Fig. S3,† a fluorescent molecular rotor sensitive to viscosity), and Mero[68–70] (Fig. S4,† both a solvatochromic dye that is sensitive to polarity and a rotor that is sensitive to viscosity).

Via sortase enzyme mediated site-specific bioconjugation[71–74] to the model protein dihydrofolate reductase (DHFR, Fig. 2b, S5 experimental details and S6 mass spectrometry for labeling efficiency†), we demonstrated all four fluorophores can report on protein aggregation with satisfactory fluorescence enhancement upon protein aggregation (Fig. 2c, CCVJ 10.9-fold, DCDHF 4.9-fold, RFP 7.8-fold, Mero 11.6-fold fluorescence enhancement). Biochemical fractionation and fluorescence imaging experiments showed that the insoluble aggregated proteins were fluorescent (Fig. 2d). Detection limits and linear range measurements demonstrated that our method is quantitative and sensitive using labeled proteins from 0.0625% to 2% in substoichiometry (Fig. 2e and S7†).

We next evaluated whether combining fluorophore-labeled DHFR proteins will lead to FRET signal upon aggregation. Spectral analyses in solvent systems ruled out CCVJ–DCDHF and CCVJ–RFP pairs due to the significant spectral overlaps (Fig. S8†). Though Mero partially overlaps with the tail of CCVJ

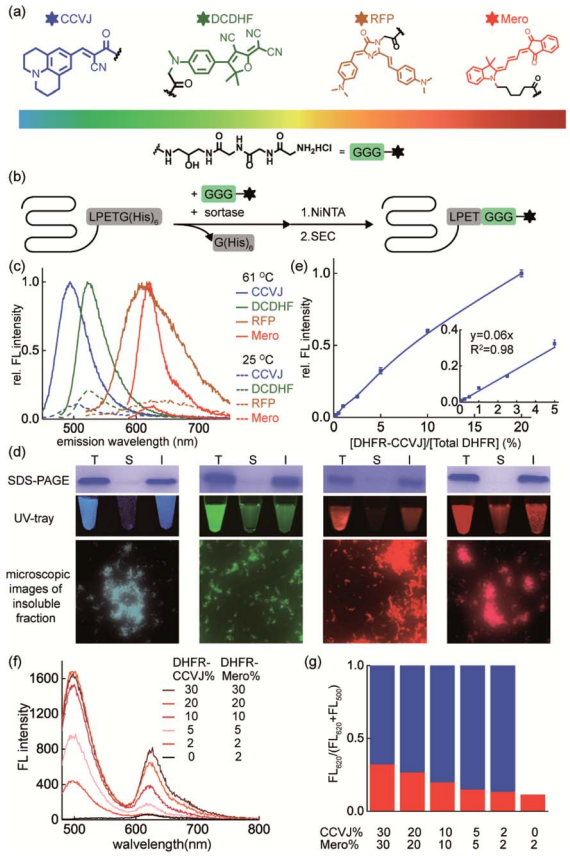

Fig. 2 A palette of environment-sensitive fluorophores reports on protein aggregation in substoichiometry. (a) Structures of protein aggregation sensors ready for bioconjugation to a protein-of-interest *via* sortase-mediated protein ligation; (b) scheme of sortase-mediated bioorthogonal conjugation of sensors to a protein-of-interest; (c) fluorescence emission spectra before and after heat induced DHFR aggregation. DHFR (50 μM, 2% labelled with sensors) was heated to 61 °C for 5 min; (d) sensors were fluorescent in the insoluble fraction of DHFR, revealed by SDS–PAGE gels and microscopic images of insoluble aggregates. (e) Stoichiometry, linear range, and lowest detection limits of CCVJ-labelled DHFR in detecting DHFR aggregation. (f) Decreasing labelled DHFR ratio minimized FRET efficiency. (g) Quantitative analysis of FRET efficiency. Blue bar: CCVJ fluorescence; Red bar: Mero fluorescence excited by CCVJ's emission. Aggregated mixture containing CCVJ- and Mero-labelled DHFR was excited at 460 nm.

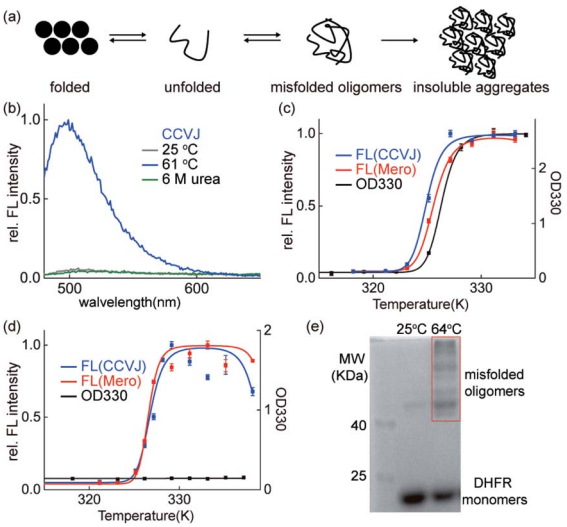

Fig. 3 Fluorescence of the protein aggregation sensors CCVJ and Mero arises from misfolded oligomers and retains in the insoluble aggregates. (a) Scheme of protein aggregation process. (b) Unfolded CCVJ-labelled DHFR was not fluorescent. DHFR (50 μM, 2% labelled with CCVJ) was unfolded by incubating in 6 M urea for 12 h. (c) Both CCVJ and Mero fluorescence from the aggregation of DHFR occur earlier than the formation of insoluble DHFR measured by the turbidity assay using OD330. DHFR (50 μM, 2% labelled, pH = 6.23). (d) Both CCVJ and Mero fluorescence were triggered by the misfolding of DHFR in the absence of insoluble DHFR. Misfolding of DHFR was induced by heating DHFR in pH neural buffer (pH = 7.40). (e) Chemical crosslinking showed the presence of misfolded oligomers.

emission spectrum, it exhibited minimal FRET effect with CCVJ, especially when Mero-labeled DHFR was in substoichiometry (Fig. 2f, g). Thus, CCVJ and Mero can serve as an orthogonal sensor pair to monitor dual-protein co-aggregation process. Together we showed that environment-sensitive fluorophores of expanded spectral coverage enabled multi-color detection of different proteins' aggregation with minimal fluorescence cross-talk.

The fluorescence arises from misfolded oligomers

Though the insoluble protein aggregates retained the fluorescence (Fig. 2d), the fluorescence of these sensors may arise from the early aggregation precursors: unfolded proteins or misfolded soluble oligomers (Fig. 3a). We next performed series of biochemical and biophysical experiments to dissect the origin of their fluorescence in detecting protein aggregation.

First, urea mediated unfolding of the DHFR-CCVJ and DHFR-Mero conjugates resulted in no fluorescence (Fig. 3b and S9†), showing that the fluorescence is not caused by unfolded proteins. Second, we used turbidity assay measured by UV-Vis spectroscopy (OD330 nm) to detect the presence of insoluble DHFR aggregates induced by heating the samples at indicated temperatures. The fluorescence signals of both CCVJ and Mero occurred at lower temperatures than the OD330 signal measuring the formation of insoluble DHFR proteins (Fig. 3c). This result suggested that the fluorescence of CCVJ and Mero may arise earlier than the formation of insoluble aggregates. Further, we found that DHFR formed no insoluble aggregates at pH 7.40 upon heating (Fig. 3d, black curve) while fluorescence was turned on (Fig. 3f, red and blue curves). In addition, we sequestered misfolded soluble oligomers of DHFR under this condition using chemical crosslinking experiment (Fig. 3e). In particular, the fluorescence intensity from misfolded oligomers was comparable to that in aggregated DHFR (Fig. S10†). Collectively, we confirmed that both CCVJ and Mero fluorescence were initially triggered by the formation of misfolded soluble oligomers and retained in insoluble aggregates. Unlike other amyloid sensors that reports on late-stage aggregated species, our sensors developed herein detected early misfolded soluble oligomers.

Dual-color thermal shift assay to quantify the interplay of thermodynamic stability during protein co-aggregation

Before using CCVJ and Mero in the dual-color mode (Fig. 4a), we first tested whether they can report on protein aggregation and quantitatively measure the melting temperature (T_m) in the single-color mode. Using DHFR protein as a model system, we quantified the melting temperatures (T_m)[51] of wild-type (WT, Fig. 4b) DHFR and mutant (Mut, M42T:H114R, Fig. 4c)[75] DHFR protein at different pHs. We observed compromised thermodynamic stability of DHFR caused by point mutations ($T_m = 325$ K for WT-DHFR and 310 K for Mut-DHFR) and increased acidity of the buffer. Importantly, swapping CCVJ and Mero for bioconjugation yielded similar melting temperatures in all cases, demonstrating the robustness of this assay in quantitative analysis (Fig. S11 and S12†).

Heterozygous mixture of both wild-type and mutant proteins widely exists in nature especially in numerous hereditary human diseases. In this regard, we combined CCVJ and Mero into a dual-color thermal shift assay to investigate how WT-DHFR and Mut-DHFR mutually influence each other during their co-aggregation process. Our dual-color thermal shift assay allowed us to simultaneously monitor the misfolding and aggregation of both WT- and Mut-DHFR proteins (Fig. 4d) and quantify their T_m values that describe the thermodynamic stability. We observed exaggerated aggregation of WT-DHFR (Fig. 4d, red dash line) in the presence of aggregated Mut-DHFR (Fig. 4d, blue dash line), which can be possibly explained by the "seeding effect" of protein aggregation. Such interplay resulted in compromised thermodynamic stability of WT-DHFR (−5.59 K) and marginal rescue of Mut-DHFR stability (0.91 K). Control experiment demonstrated the fluorescence turn-on of Mut-DHFR-Mero requires both the self-aggregation of Mut-DHFR-Mero and the co-aggregation of surrounding unlabeled proteins (Fig. S13 and S14†).

To demonstrate the technical advantages of our assay, we included the commercial single-color thermal shift assay using SYPRO® orange dye and PROTEOSTAT® dye in parallel control experiments. Both dyes detect protein misfolding and aggregation by non-covalently binding to any aggregated proteins without protein selectivity (Fig. 4e). Such mechanism-of-action differs from our bioorthogonal covalent conjugation of sensor and thus prevents them from being used to resolve the thermodynamic profiles of different proteins. Both dyes provided a biased thermal shift curve in detecting protein co-aggregation of WT-DHFR and mut-DHFR (Fig. 4f and g, black curves). However, these commercial methods provided similar T_m values in the single pure protein mode as in our assay (Fig. 4d *vs.* f and g, solid red and blue curves), validating the robustness of our method. Moreover, the overlapped fluorescence spectra of both dyes (Fig. 4h) further impedes their applications in detecting protein co-aggregations due to the lack of signal orthogonality. Finally, combined addition of both dyes failed to resolve protein co-aggregation (Fig. 4i). These results clearly showed the advantages of our assay in comparison to the commercial single-color thermal shift assay.

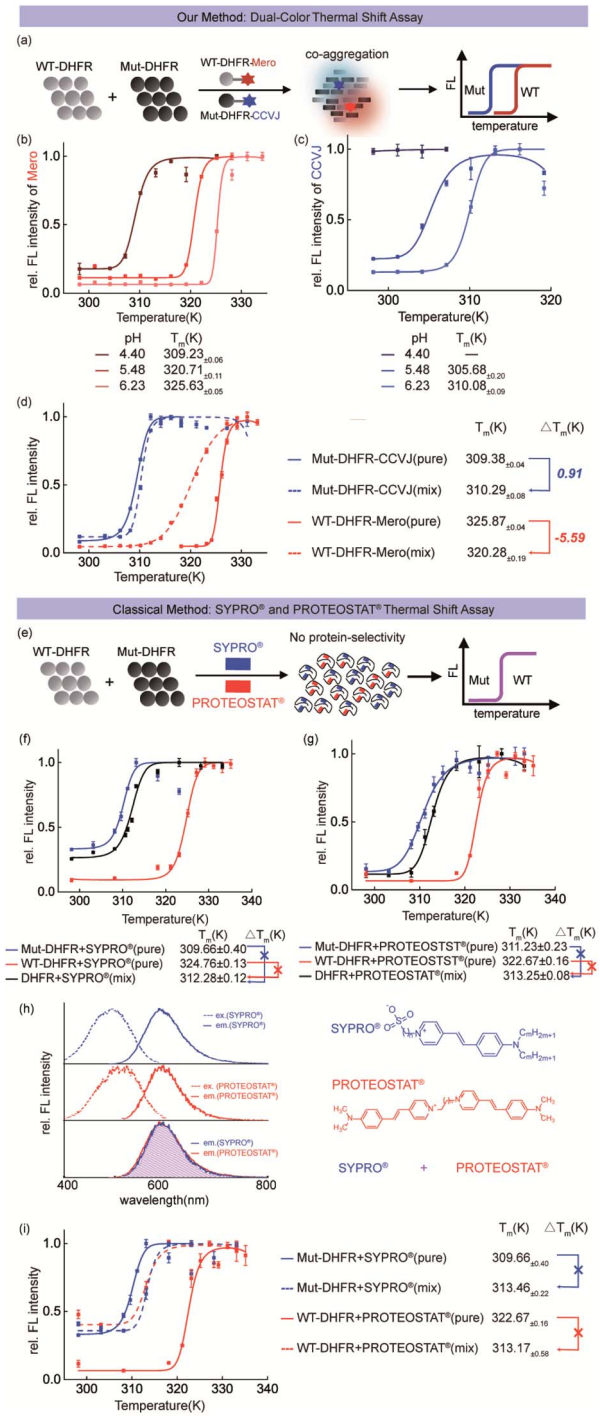

Fig. 4 Dual-color thermal shift assay to quantify the interplay of thermodynamic stability during protein co-aggregation. (a) Experiment scheme. (b and c) pH dependent thermodynamic stability of WT-DHFR and Mut-DHFR quantified by our assay. (d) Dual-color thermal shift assay to monitor protein co-aggregation of WT-DHFR and Mut-DHFR and quantify the interplay of thermodynamic stability. (e) Experiment scheme of SYPRO® and PROTEOSTAT® single color thermal shift assay. (f) Commercial SYPRO® thermal shift assay does not resolve two proteins' co-aggregation. (g) Commercial PROTEOSTAT® thermal shift assay does not resolve two proteins' co-aggregation. (h) Spectral overlaps between SYPRO® and PROTEOSTAT® prevent them from being used together. (i) Combined utilization of SYPRO® and PROTEOSTAT® cannot resolve the co-aggregation process of two different proteins due to the lack of signal orthogonality.

The complexity of protein co-aggregation in transthyretin amyloidosis

Transthyretin (TTR) is a homo-tetrameric protein in human blood plasma whose pathogenic mutations lead to hereditary amyloidosis, such as familiar polyneuropathy and senile cardiomyopathy. Intriguingly, multiple lines of clinical evidence have demonstrated the co-aggregation or co-deposition of pathogenic TTR amyloids and other amyloidogenic proteins, such as light chain, apolipoprotein A-IV, and serum amyloid A proteins (Fig. 5a).[76–82] These pathological results lead to a biochemical question: what is the individual function of these co-aggregated proteins? To partially examine this question and demonstrate the application of our dual-color thermal shift assay in clinical scenarios, we selected transthyretin (TTR) and apolipoprotein A–IV (APOA4) as a pair of model proteins based on the clinical diagnosis results.[83,84] We recombinantly prepared TTR and APOA4 proteins, characterized their structural features and labeled them with CCVJ and Mero fluorophores (Fig. S15†). We aimed to show how APOA4 protein influences the aggregation of TTR in a co-aggregation experiment (Fig. 5b). We found that the presence of aggregated APOA4 protein can slightly stabilized TTR mutant and inhibit its aggregation (Fig. 5c), suggesting its role as a pathological chaperone (Fig. S15e and S16†). This observation echoes the effect of apolipoprotein E in Alzheimer's disease widely reported in literature and may deserve further biochemical analysis.[85–88]

Oligomeric proteins that involve subunit exchange between wild-type and mutant proteins in a heterozygous mixture pose further technical challenge to study the co-aggregation process and the interplay in the thermodynamic stability. In particular, patients carrying pathogenic TTR mutations are often heterozygous. Using TTR as a model system, we investigated how the thermodynamic stabilities of heterozygous mixture after subunit exchange fluctuated during heat induced co-aggregation (Fig. 5d and e). Similar with the monomeric DHFR scenario, WT-TTR was destabilized thermodynamically in the presence of Mut-TTR (−3.52 K) but Mut-TTR (L55P) was slightly rescued by WT-TTR (1.17 K) during co-aggregation. This observation deviates from the fact that TTR's kinetic stability can be significantly enhanced by subunit exchange with a stable mutant as TTR aggregation is kinetically controlled by the rate-limiting tetramer dissociation step. The TTR results highlighted the difference in protein thermodynamic and kinetic stability. To further study the impact of small molecule ligands on the thermodynamic stability during protein co-aggregation process, we utilized the recently FDA-approved kinetic stabilizer Tafamidis[89] (Fig. S17†). We observed marginal thermodynamic stabilization effect by Tafamidis at substoichiometric concentration, and significant stabilization of both WT- and Mut-TTR at stoichiometric concentration. This observation can be explained by the fact that Tafamidis as a kinetic stabilizer controls the tetramer dissociation step and only takes secondary effect on the thermodynamic stability of monomeric TTR after dissociation. In this case, our results highlighted the significance of distinguishing whether the stabilizing effect of a ligand is driven by the kinetic or thermodynamic factors of the target proteins.

Overall, these results together demonstrated the assay developed herein can provide biochemical evidence to partially support and explain the complex clinical observations.

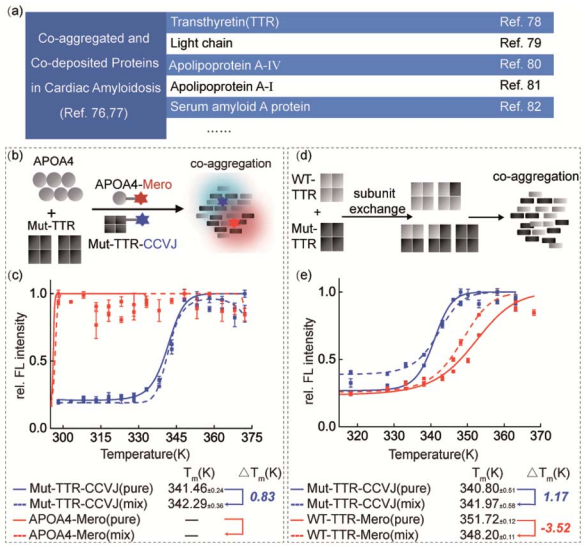

Fig. 5 The complexity of protein co-aggregation in transthyretin amyloidosis. (a) Clinical and literature reported co-deposited proteins in cardiac amyloidosis. (b) Experimental scheme of TTR and APOA4 protein co-aggregation. (c) Aggregated APOA4 slightly stabilized TTR (L55P) mutant and inhibited its aggregation. (d) Subunit exchange of WT-TTR and TTR (L55P) mutant. (e) Dual-color thermal shift assay to monitor protein co-aggregation of tetrameric WT-TTR and Mut-TTR proteins with subunit exchange and quantify the interplay in thermodynamic stability.

Dual-color thermal shift assay to evaluate drug stabilization effect on protein co-aggregation

Thermal shift assay provides quantitative analysis of shifts in protein thermodynamic stability upon binding to ligands. In this work, we further evaluated how small molecule ligands interfere with protein co-aggregation process *via* our dual-color thermal shift assay (Fig. 6a).

First, in the single-color mode, we demonstrated our assay is capable of quantifying the dose-dependent stabilization of DHFR by its known inhibitor trimethoprim (TMP, Fig. 6b). Second, we examined how TMP differentially stabilizes WT-DHFR and Mut-DHFR, namely the partition of ligands in this heterozygous model system. We observed that at sub-stoichiometric concentration, TMP stabilized both WT- and Mut-DHFR to the similar extent (Fig. 6c, 9.47 K for WT, 9.29 K for Mut). However, when the ligand was in excess, TMP can stabilize Mut-DHFR to a larger extent than WT-DHFR (Fig. 6d, 13.50 K for Mut, 11.44 K for WT). However, in both scenarios, Mut-DHFR cannot be stabilized to the same stability as WT-DHFR when they were both stabilized by TMP. Again, such observation was not possible using the current single-color thermal shift assay by the SYPRO® orange dye (Fig. 6e). Finally, we evaluated how a ligand selectively engages into two

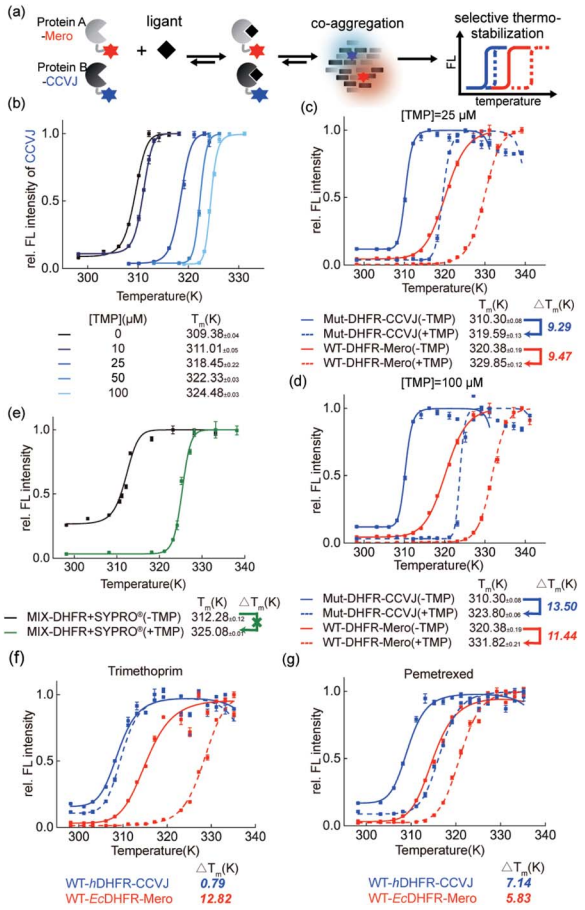

Fig. 6 Ligand effect on the protein co-aggregation process and thermodynamic stability. (a) Experiment scheme. (b) Dose dependent stabilization of Mut-DHFR by TMP using our assay in the single-color mode. (c and d) Dual-color mode revealed differential ligand stabilizing effect on the co-aggregation of WT- and Mut-DHFR in sub or excess stoichiometry. (e) Commercial single-color thermal shift assay is not capable of studying co-aggregation system. (f and g) Selective stabilizing effect of different drug ligands on the co-aggregation of hDHFR and EcDHFR.

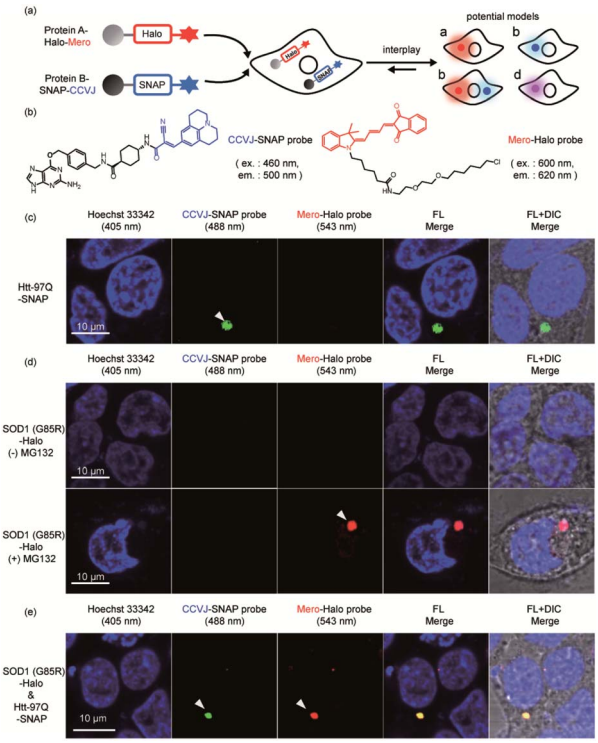

Fig. 7 Visualization of protein co-aggregation in live cells. (a) Experiment scheme and potential outcomes. (b) Structures of Mero-Halo and CCVJ-SNAP probes. (c) CCVJ detected the aggregation of Htt-97Q-SNAP protein in live cells. (d) Mero detected the aggregation of SOD1(G85R)-Halo upon inhibition of proteosome by MG132. (e) Htt-97Q-SNAP co-aggregated with SOD1(G85R)-Halo even without MG132 inhibition. Green: CCVJ fluorescence, 488 nm channel. Red: Mero fluorescence, 543 nm channel.

homologous proteins from different organisms. Using human DHFR (hDHFR) and the abovementioned *E. coli* DHFR (EcDHFR) as a model system, we found that TMP as an antibiotic drug is extremely selective to EcDHFR (Fig. 6f), whereas pemetrexed as a chemotherapy reagent partitioned into hDHFR more than EcDHFR (Fig. 6g).

The interplay during protein co-aggregation in live cells

Finally, we extended our study into the complex cellular milieu to demonstrate these sensors are compatible with cellular applications. Sortase mediated protein ligation we used in this work is not compatible with cellular environment. Using the reported AggTag method, we approached to SNAP-Tag and Halo-Tag technologies for the bioorthogonal conjugation of CCVJ and Mero sensors towards two different POIs (Fig. 7a and b).[57] We first demonstrated these two sensors can selectively detect single protein aggregation in live cells. In HEK293T cells transiently expressing Htt-97Q-SNAP whose aggregation leads to Huntington's disease,[90,91] CCVJ-SNAP probe detected perinuclear puncta (Fig. 7c, 488 nm channel). In addition, proteasome inhibitor MG132 induced protein degradation attenuation resulted in the accumulation of SOD1 (G85R) -Halo aggregates in the cell,[92] which was visualized by Mero-Halo probe (Fig. 7d, 543 nm channel). Interestingly, with sufficient degradation capacity, even mutant SOD1 can be degraded properly and did not accumulate in its aggregated state (Fig. 7d, upper panel). However, dual-color imaging experiment revealed that co-expression of Htt-97Q-SNAP together with SOD1 (G85R) -Halo proteins in HEK293T cells caused co-aggregation of both SOD1 (G85R) and Htt-97Q proteins in the perinuclear region of the cell (Fig. 7e). These results indicated that the aggregation of Htt-97Q may saturate the cellular degradation capacity and intoxicate the degradation of SOD1 (G85R) mutant, leading to the co-aggregation of both proteins. Different from the buffer environment, protein co-aggregation may influence each other by sharing the same protein quality control machineries and pathways. Together, these results demonstrated that the multi-color protein aggregation sensors developed here not only quantify changes in thermodynamic stability in buffer (Fig. 4 and 6) but also detect protein co-aggregation in live cells (Fig. 7).

Conclusions

In summary, we have demonstrated how to repurpose environment-sensitive fluorophores to detect two proteins' aggregation *via* bioorthogonal labeling. Our dual-color thermal shift assay developed in this work allowed for orthogonal and quantitative study of protein co-aggregation process, which was impossible if using the commercial single-color thermal shift assay. Different from all previous kinetics studies, our work provided the first quantitative analysis on the thermodynamic interplay during protein co-aggregation. Future color enrichment of the sensor toolbox by developing novel protein aggregation sensors from solvatochromic fluorophores, fluorescent molecular rotors, and AIEgens may improve the detection multiplexity for more complex disease model systems, such as amyotrophic lateral sclerosis disease.[93–95]

Data availability

Supplementary figures, experimental methods, and synthetic characterizations can be found in the supplementary information.

Author contributions

Y. Liu and W. Wan conceptualized the project and edited the manuscript. Y. Bai performed the experiments, analyzed the data, and wrote the original draft. W. Jin, Y. Huang, H. Lyu, and Q. Xia provided experimental resources. X. Dong and Z. Gao helped with data analysis.

Conflicts of interest

There are no conflicts to declare.

Acknowledgements

This work was supported, in part, by funds from National Natural Science Foundation of China (21907091), the LiaoNing Revitalization Talents Program from the Liaoning province of China (XLYC1907048), China Postdoctoral Science Foundation Grant (2019M661138), Pfizer ASPIRE award for transthyretin amyloidosis basic research.

Notes and references

1 F. Chiti and C. M. Dobson, *Annu. Rev. Biochem.*, 2017, **86**, 27–68.
2 F. U. Hartl, *Annu. Rev. Biochem.*, 2017, **86**, 21–26.
3 W. E. Balch, R. I. Morimoto, A. Dillin and J. W. Kelly, *Science*, 2008, **319**, 916–919.
4 C. A. De Carufel, N. Quittot, P. T. Nguyen and S. Bourgault, *Angew. Chem., Int. Ed. Engl.*, 2015, **54**, 14383–14387.
5 Y. S. Eisele, C. Monteiro, C. Fearns, S. E. Encalada, R. L. Wiseman, E. T. Powers and J. W. Kelly, *Nat. Rev. Drug Discovery*, 2015, **14**, 759–780.
6 L. M. Young, L. H. Tu, D. P. Raleigh, A. E. Ashcroft and S. E. Radford, *Chem. Sci.*, 2017, **8**, 5030–5040.
7 C. J. Sarell, P. G. Stockley and S. E. Radford, *Prion*, 2013, **7**, 359–368.
8 C. J. Sarell, L. A. Woods, Y. C. Su, G. T. Debelouchina, A. E. Ashcroft, R. G. Griffin, P. G. Stockley and S. E. Radford, *J. Biol. Chem.*, 2013, **288**, 7327–7337.
9 L. M. Young, R. A. Mahood, J. C. Saunders, L. H. Tu, D. P. Raleigh, S. E. Radford and A. E. Ashcroft, *Analyst*, 2015, **14**, 6990–6999.
10 T. Doussineau, C. Mathevon, L. Altamura, C. Vendrely, P. Dugourd, V. Forge and R. Antoine, *Angew. Chem., Int. Ed.*, 2016, **55**, 2340–2344.
11 A. Aliyan, N. P. Cook and A. A. Marti, *Chem. Rev.*, 2019, **119**, 11819–11856.
12 G. S. Loving, M. Sainlos and B. Imperiali, *Trends Biotechnol.*, 2010, **28**, 73–83.
13 A. S. Klymchenko, *Acc. Chem. Res.*, 2017, **50**, 366–375.
14 M. Lindgren, K. Sorgjerd and P. Hammarstrom, *Biophys. J.*, 2005, **88**, 4200–4212.
15 L. H. Qin, J. Vastl and J. M. Gao, *Mol. BioSyst.*, 2010, **6**, 1791–1795.
16 J. Sutharsan, M. Dakanali, C. C. Capule, M. A. Haidekker, J. Yang and E. A. Theodorakis, *ChemMedChem*, 2010, **5**, 56–60.
17 Y. Hong, J. W. Lam and B. Z. Tang, *Chem. Commun.*, 2009, 4332–4353, DOI: 10.1039/b904665h.
18 Y. Hong, L. Meng, S. Chen, C. W. Leung, L. T. Da, M. Faisal, D. A. Silva, J. Liu, J. W. Lam, X. Huang and B. Z. Tang, *J. Am. Chem. Soc.*, 2012, **134**, 1680–1689.
19 W. Fu, C. Yan, Z. Guo, J. Zhang, H. Zhang, H. Tian and W. H. Zhu, *J. Am. Chem. Soc.*, 2019, **141**, 3171–3177.
20 C. Wu, Z. Wang, H. Lei, Y. Duan, M. T. Bowers and J. E. Shea, *J. Mol. Biol.*, 2008, **384**, 718–729.
21 W. G. Yang, Y. Wong, O. T. W. Ng, L. P. Bai, D. W. J. Kwong, Y. Ke, Z. H. Jiang, H. W. Li, K. K. L. Yung and M. S. Wong, *Angew. Chem., Int. Ed.*, 2012, **51**, 1804–1810.
22 K. P. R. Nilsson, M. Lindgren and P. Hammarstrom, *Methods Mol. Biol.*, 2018, **1779**, 485–496.
23 J. Y. Kim, S. Sahu, Y. H. Yau, X. Wang, S. G. Shochat, P. H. Nielsen, M. S. Dueholm, D. E. Otzen, J. Lee, M. M. Delos Santos, J. K. Yam, N. Y. Kang, S. J. Park, H. Kwon, T. Seviour, L. Yang, M. Givskov and Y. T. Chang, *J. Am. Chem. Soc.*, 2016, **138**, 402–407.
24 M. Z. Chen, N. S. Moily, J. L. Bridgford, R. J. Wood, M. Radwan, T. A. Smith, Z. G. Song, B. Z. Tang, L. Tilley, X. H. Xu, G. E. Reid, M. A. Pouladi, Y. N. Hong and D. M. Hatters, *Nat. Commun.*, 2017, **8**, 474.
25 T. C. Owyong, P. Subedi, J. Deng, E. Hinde, J. J. Paxman, J. M. White, W. Chen, B. Heras, W. W. H. Wong and Y. Hong, *Angew. Chem., Int. Ed. Engl.*, 2020, **59**, 10129–10135.
26 A. A. Shemetov, I. Nabiev and A. Sukhanova, *ACS Nano*, 2012, **6**, 4585–4602.
27 A. Iscen, C. R. Brue, K. F. Roberts, J. Kim, G. C. Schatz and T. J. Meade, *J. Am. Chem. Soc.*, 2019, **141**, 16685–16695.

28 N. Bandara, A. K. Sharma, S. Krieger, J. W. Schultz, B. H. Han, B. E. Rogers and L. M. Mirica, *J. Am. Chem. Soc.*, 2017, **139**, 12550–12558.
29 B. Jiang, A. Aliyan, N. P. Cook, A. Augustine, G. Bhak, R. Maldonado, A. D. S. McWilliams, E. M. Flores, N. Mendez, M. Shahnawaz, F. J. Godoy, J. Montenegro, I. Moreno-Gonzalez and A. A. Marti, *J. Am. Chem. Soc.*, 2019, **141**, 15605–15610.
30 P. R. Banerjee and A. A. Deniz, *Chem. Soc. Rev.*, 2014, **43**, 1172–1188.
31 P. R. Banerjee, D. M. Mitrea, R. W. Kriwacki and A. A. Deniz, *Angew. Chem., Int. Ed. Engl.*, 2016, **55**, 1675–1679.
32 A. C. Ferreon, C. R. Moran, J. C. Ferreon and A. A. Deniz, *Angew. Chem., Int. Ed. Engl.*, 2010, **49**, 3469–3472.
33 L. Mayne and S. W. Englander, *Protein Sci.*, 2000, **9**, 1873–1877.
34 M. M. Krishna and S. W. Englander, *Protein Sci.*, 2007, **16**, 449–464.
35 J. J. Skinner, W. K. Lim, S. Bedard, B. E. Black and S. W. Englander, *Protein Sci.*, 2012, **21**, 996–1005.
36 S. W. Englander and L. Mayne, *Proc. Natl. Acad. Sci. U. S. A.*, 2014, **111**, 15873–15880.
37 A. M. Last and C. V. Robinson, *Curr. Opin. Chem. Biol.*, 1999, **3**, 564–570.
38 J. A. Aquilina and C. V. Robinson, *Biochem. J.*, 2003, **375**, 323–328.
39 J. T. Hopper and C. V. Robinson, *Angew. Chem., Int. Ed. Engl.*, 2014, **53**, 14002–14015.
40 T. M. Allison, E. Reading, I. Liko, A. J. Baldwin, A. Laganowsky and C. V. Robinson, *Nat. Commun.*, 2015, **6**, 8551.
41 G. Nubling, B. Bader, J. Levin, J. Hildebrandt, H. Kretzschmar and A. Giese, *Mol. Neurodegener.*, 2012, **7**, 35.
42 A. A. Rubel, T. A. Ryzhova, K. S. Antonets, Y. O. Chernoff and A. Galkin, *Prion*, 2013, **7**, 469–476.
43 U. B. Ericsson, B. M. Hallberg, G. T. Detitta, N. Dekker and P. Nordlund, *Anal. Biochem.*, 2006, **357**, 289–298.
44 J. A. Irving, I. Haq, J. A. Dickens, S. V. Faull and D. A. Lomas, *Biochem. J.*, 2014, **460**, 103–115.
45 C. J. Layton and H. W. Hellinga, *Protein Sci.*, 2011, **20**, 1439–1450.
46 M. Vedadi, F. H. Niesen, A. Allali-Hassani, O. Y. Fedorov, P. J. Finerty Jr, G. A. Wasney, R. Yeung, C. Arrowsmith, L. J. Ball, H. Berglund, R. Hui, B. D. Marsden, P. Nordlund, M. Sundstrom, J. Weigelt and A. M. Edwards, *Proc. Natl. Acad. Sci. U. S. A.*, 2006, **103**, 15835–15840.
47 L. Dai, N. Prabhu, L. Y. Yu, S. Bacanu, A. D. Ramos and P. Nordlund, *Annu. Rev. Biochem.*, 2019, **88**, 383–408.
48 D. Martinez Molina, R. Jafari, M. Ignatushchenko, T. Seki, E. A. Larsson, C. Dan, L. Sreekumar, Y. Cao and P. Nordlund, *Science*, 2013, **341**, 84–87.
49 S. E. Giuliani, A. M. Frank and F. R. Collart, *Biochemistry*, 2008, **47**, 13974–13984.
50 J. J. Lavinder, S. B. Hari, B. J. Sullivan and T. J. Magliery, *J. Am. Chem. Soc.*, 2009, **131**, 3794–3795.
51 M. C. Lo, A. Aulabaugh, G. Jin, R. Cowling, J. Bard, M. Malamas and G. Ellestad, *Anal. Biochem.*, 2004, **332**, 153–159.
52 J. O. Esteves-Villanueva, H. Trzeciakiewicz, D. A. Loeffler and S. Martic, *Biochemistry*, 2015, **54**, 293–302.
53 D. Laor, D. Sade, S. Shaham-Niv, D. Zaguri, M. Gartner, V. Basavalingappa, A. Raveh, E. Pichinuk, H. Engei, K. Lwasaki, T. Yamamoto, H. Noothalapati and E. Gazit, *Nat. Commun.*, 2019, **10**, 62.
54 S. Navarro and S. Ventura, *Biotechnol. J.*, 2014, **9**, 1259–1266.
55 C. M. Haney, C. L. Cleveland, R. F. Wissner, L. Owei, J. Robustelli, M. J. Daniels, M. Canyurt, P. Rodriguez, H. Ischiropoulos, T. Baumgart and E. J. Petersson, *Biochemistry*, 2017, **56**, 683–691.
56 J. V. Jun, C. M. Haney, R. J. Karpowicz, S. Giannakoulias, V. M. Y. Lee, E. J. Petersson and D. M. Chenoweth, *J. Am. Chem. Soc.*, 2019, **141**, 1893–1897.
57 C. M. Haney, R. F. Wissner, J. B. Warner, Y. J. Wang, J. J. Ferrie, J. C. Dustin, R. J. Karpowicz, V. M. Lee and E. J. Petersson, *Org. Biomol. Chem.*, 2016, **14**, 1584–1592.
58 K. H. Jung, S. F. Kim, Y. Liu and X. Zhang, *ChemBioChem*, 2019, **20**, 1078–1087.
59 Y. Liu, C. H. Wolstenholme, G. C. Carter, H. Liu, H. Hu, L. S. Grainger, K. Miao, M. Fares, C. A. Hoelzel, H. P. Yennawar, G. Ning, M. Du, L. Bai, X. Li and X. Zhang, *J. Am. Chem. Soc.*, 2018, **140**, 7381–7384.
60 C. H. Wolstenholme, H. Hu, S. Ye, B. E. Funk, D. Jain, C. H. Hsiung, G. Ning, Y. Liu, X. Li and X. Zhang, *J. Am. Chem. Soc.*, 2020, **142**, 17515–17523.
61 S. Ye, H. Zhang, J. Fei, C. H. Wolstenholme and X. Zhang, *Angew. Chem., Int. Ed. Engl.*, 2020, **60**, 1339–1346.
62 Y. Liu, K. Miao, Y. H. Li, M. Fares, S. Y. Chen and X. Zhang, *Biochemistry*, 2018, **57**, 4663–4674.
63 M. Fares, Y. Li, Y. Liu, K. Miao, Z. Gao, Y. Zhai and X. Zhang, *Bioconjug. Chem.*, 2018, **29**, 215–224.
64 H. L. D. Lee, S. J. Lord, S. Iwanaga, K. Zhan, H. X. Xie, J. C. Williams, H. Wang, G. R. Bowman, E. D. Goley, L. Shapiro, R. J. Twieg, J. H. Rao and W. E. Moerner, *J. Am. Chem. Soc.*, 2010, **132**, 15099–15101.
65 T. Suhina, B. Weber, C. E. Carpentier, K. Lorincz, P. Schall, D. Bonn and A. M. Brouwer, *Angew. Chem., Int. Ed.*, 2015, **54**, 3688–3691.
66 G. Feng, C. Luo, H. Yi, L. Yuan, B. Lin, X. Luo, X. Hu, H. Wang, C. Lei, Z. Nie and S. Yao, *Nucleic Acids Res.*, 2017, **45**, 10380–10392.
67 J. S. Paige, K. Y. Wu and S. R. Jaffrey, *Science*, 2011, **333**, 642–646.
68 C. J. MacNevin, D. Gremyachinskiy, C. W. Hsu, L. Li, M. Rougie, T. T. Davis and K. M. Hahn, *Bioconjug. Chem.*, 2013, **24**, 215–223.
69 C. J. MacNevin, A. Toutchkine, D. J. Marston, C. W. Hsu, D. Tsygankov, L. Li, B. Liu, T. Qi, D. V. Nguyen and K. M. Hahn, *J. Am. Chem. Soc.*, 2016, **138**, 2571–2575.
70 C. J. MacNeyin, T. Watanabe, M. Weitzman, A. Gulyani, S. Fuehrer, N. K. Pinkin, X. Tian, F. Liu, J. Jin and K. M. Hahn, *J. Am. Chem. Soc.*, 2019, **141**, 7275–7282.

71 C. P. Guimaraes, M. D. Witte, C. S. Theile, G. Bozkurt, L. Kundrat, A. E. M. Blom and H. L. Ploegh, *Nat. Protoc.*, 2013, **8**, 1787–1799.
72 Y. M. Li, Y. T. Li, M. Pan, X. Q. Kong, Y. C. Huang, Z. Y. Hong and L. Liu, *Angew. Chem., Int. Ed.*, 2014, **53**, 2198–2202.
73 M. W. Popp and H. L. Ploegh, *Angew. Chem., Int. Ed. Engl.*, 2011, **50**, 5024–5032.
74 H. H. Wang, B. Altun, K. Nwe and A. Tsourkas, *Angew. Chem., Int. Ed. Engl.*, 2017, **56**, 5349–5352.
75 Y. Cho, X. Zhang, K. F. Pobre, Y. Liu, D. L. Powers, J. W. Kelly, L. M. Gierasch and E. T. Powers, *Cell Rep.*, 2015, **11**, 321–333.
76 P. Garcia-Pavia, C. Rapezzi, Y. Adler, M. Arad, C. Basso, A. Brucato, I. Burazor, A. L. P. Caforio, T. Damy, U. Eriksson, M. Fontana, J. D. Gillmore, E. Gonzalez-Lopez, M. Grogan, S. Heymans, M. Imazio, I. Kindermann, A. V. Kristen, M. S. Maurer, G. Merlini, A. Pantazis, S. Pankuweit, A. G. Rigopoulos and A. Linhart, *Eur. Heart J.*, 2021, **42**, 1554–1568.
77 M. S. Maurer, P. Elliott, R. Comenzo, M. Semigran and C. Rapezzi, *Circulation*, 2017, **135**, 1357–1377.
78 F. L. Ruberg and J. L. Berk, *Circulation*, 2012, **126**, 1286–1300.
79 M. Grogan, A. Dispenzieri and M. A. Gertz, *Heart*, 2017, **103**, 1065–1072.
80 L. Obici, M. Nuvolone and G. Merlini, *Kidney Int.*, 2016, **90**, 479–481.
81 T. Joy, J. Wang, A. Hahn and R. A. Hegele, *Clin. Biochem.*, 2003, **36**, 641–645.
82 H. J. Lachmann, H. J. Goodman, J. A. Gilbertson, J. R. Gallimore, C. A. Sabin, J. D. Gillmore and P. N. Hawkins, *N. Engl. J. Med.*, 2007, **356**, 2361–2371.
83 J. Bergstrom, C. Murphy, M. Eulitz, D. T. Weiss, G. T. Westermark, A. Solomon and P. Westermark, *Biochem. Biophys. Res. Commun.*, 2001, **285**, 903–908.
84 J. Bergstrom, C. L. Murphy, D. T. Weiss, A. Solomon, K. Sletten, U. Hellman and P. Westermark, *Lab. Invest.*, 2004, **84**, 981–988.
85 T. Wisniewski and B. Frangione, *Neurosci. Lett.*, 1992, **135**, 235–238.
86 J. C. Genereux, S. Qu, M. Zhou, L. M. Ryno, S. Wang, M. D. Shoulders, R. J. Kaufman, C. I. Lasmezas, J. W. Kelly and R. L. Wiseman, *EMBO J.*, 2015, **34**, 4–19.
87 K. C. Chen, S. Qu, S. Chowdhury, I. C. Noxon, J. D. Schonhoft, L. Plate, E. T. Powers, J. W. Kelly, G. C. Lander and R. L. Wiseman, *EMBO J.*, 2017, **36**, 2296–2309.
88 I. Gallotta, A. Sandhu, M. Peters, M. Haslbeck, R. Jung, S. Agilkaya, J. L. Blersch, C. Rodelsperger, W. Roseler, C. Huang, R. J. Sommer and D. C. David, *Nature*, 2020, **584**, 410–414.
89 H. Razavi, S. K. Palaninathan, E. T. Powers, R. L. Wiseman, H. E. Purkey, N. N. Mohamedmohaideen, S. Deechongkit, K. P. Chiang, M. T. A. Dendle, J. C. Sacchettini and J. W. Kelly, *Angew. Chem., Int. Ed.*, 2003, **42**, 2758–2761.
90 S. Tomoshige, S. Nomura, K. Ohgane, Y. Hashimoto and M. Ishikawa, *Angew. Chem., Int. Ed.*, 2017, **56**, 11530–11533.
91 A. Ansaloni, Z. M. Wang, J. S. Jeong, F. S. Ruggeri, G. Dietler and H. A. Lashuel, *Angew. Chem., Int. Ed. Engl.*, 2014, **53**, 1928–1933.
92 L. I. Bruijn, M. W. Becher, M. K. Lee, K. L. Anderson, N. A. Jenkins, N. G. Copeland, S. S. Sisodia, J. D. Rothstein, D. R. Borchelt, D. L. Price and D. W. Cleveland, *Neuron*, 1997, **18**, 327–338.
93 A. Loredo, J. Tang, L. S. Wang, K. L. Wu, Z. Peng and H. Xiao, *Chem. Sci.*, 2020, **11**, 4410–4415.
94 J. Tang, M. A. Robichaux, K. L. Wu, J. Pei, N. T. Nguyen, Y. Zhou, T. G. Wensel and H. Xiao, *J. Am. Chem. Soc.*, 2019, **141**, 14699–14706.
95 J. Tang, L. S. Wang, A. Loredo, C. Cole and H. Xiao, *Chem. Sci.*, 2020, **11**, 6701–6708.